

# Electronic and optical properties of $\beta'$ -Tb<sub>2</sub>(MoO<sub>4</sub>)<sub>3</sub>: DFT+U approach

A.H. Reshak<sup>1,2,a</sup>

<sup>1</sup> New Technologies – Research Centre, University of West Bohemia, Univerzitni 8, 306 14 Pilsen, Czech Republic

<sup>2</sup> School of Material Engineering, University Malaysia Perlis, 01007 Kangar, Perlis, Malaysia

Received 13 July 2016 / Received in final form 31 August 2016

Published online 28 November 2016 – © EDP Sciences, Società Italiana di Fisica, Springer-Verlag 2016

**Abstract.** The ground state properties of  $\beta'$ -Tb<sub>2</sub>(MoO<sub>4</sub>)<sub>3</sub> are investigated using the density functional theory plus U-Hubbard Hamiltonian. To ascertain the influence of the spin-polarization on the ground state properties of orthorhombic  $\beta'$ -Tb<sub>2</sub>(MoO<sub>4</sub>)<sub>3</sub>, we have performed spin-polarization calculations and the spin-polarized electronic band structure for spin-up ( $\uparrow$ ) and spin-down ( $\downarrow$ ) are calculated. It has been found that for spin-up ( $\uparrow$ ) and spin-down ( $\downarrow$ ) the  $\beta'$ -Tb<sub>2</sub>(MoO<sub>4</sub>)<sub>3</sub> compound possesses indirect energy band gap, as the valence band maximum (VBM) is located at *Y* point of the Brillouin zone (BZ) and the conduction band minimum (CBM) at the center of the BZ. The calculated value of the band gap is 3.61 eV for spin-up ( $\uparrow$ ) and spin-down ( $\downarrow$ ), and it is in close agreement with the measured one (3.76 eV). It is clear that the electronic band structure for spin-up ( $\uparrow$ ) and spin-down ( $\downarrow$ ) cases presents identical configuration. Therefore, we can conclude that the spin-polarization has identical influence on the ground state properties of  $\beta'$ -Tb<sub>2</sub>(MoO<sub>4</sub>)<sub>3</sub>. To ascertain this observation, we have presented and explained the necessary ingredients of the calculated total and atom-resolved density of states. It has been noticed that the calculated total density of states (TDOS) for spin-up ( $\uparrow$ ) and spin-down ( $\downarrow$ ) cases are identical confirming that the spin-polarization has identical influence on the ground state properties of  $\beta'$ -Tb<sub>2</sub>(MoO<sub>4</sub>)<sub>3</sub>. For more details, in order to have deep insight into the electronic structure, we have presented the atom-resolved density of states which show identical features for spin-up ( $\uparrow$ ) and spin-down ( $\downarrow$ ). The angular momentum projected density of states (PDOS) helps to identify the angular momentum character of the various structures. To obtain more details about the electronic structure and, hence, the ground state properties, the complex first-order linear optical dispersion is calculated for spin-up ( $\uparrow$ ) and spin-down ( $\downarrow$ ) cases to ascertain the influence of the spin-polarization on the ground state properties.

## 1 Introduction

Because of their valuable properties, molybdate crystals have become considerable candidates for practical applications in photonic, laser, thermoelectric and electronic technologies [1–8]. Molybdates containing rare-earth ions gain special attention due to their potential application as laser and luminescent hosts [6–16]. In molybdates, the rare-earth ions occupied low-symmetry positions which is the main factor for the creation of efficient luminescent media. It is interesting to mention that rare-earth molybdates can be obtained in the form of large single crystals of high optical quality, characterized by high mechanical resistance, great resistance to external factors, and interesting elastic and electric properties [17]. Among the rare-earth molybdates is terbium molybdate in  $\beta'$ -phase,  $\beta'$ -Tb<sub>2</sub>(MoO<sub>4</sub>)<sub>3</sub> ( $\beta'$ -TMO).  $\beta'$ -TMO is a fully coupled ferroelectric-ferroelastic crystal and it is a widely noticed material in addition to

Gd<sub>2</sub>(MoO<sub>4</sub>)<sub>3</sub> [18,19]. The transmission spectrum of  $\beta'$ -TMO shows the energy band gap of about 3.76 eV [20] and the  $\beta'$ -TMO crystals are transparent over the range of about 340–1750 nm. The molybdates possess a sequence of the phase transitions with a temperature variation, and the  $\beta$  and  $\beta'$  polymorph modifications are noncentrosymmetric [21–25]. The  $\beta'$ -Tb<sub>2</sub>(MoO<sub>4</sub>)<sub>3</sub> phase crystallizes in orthorhombic symmetry with Pba2 space group at temperature below 433 K [24,25]. The lattice parameters are  $a = 10.35387(6)$  Å,  $b = 10.38413(6)$  Å,  $c = 10.65695(7)$  Å and  $V = 1145.79(1)$  Å<sup>3</sup> [26]. It is known that three different types of (MoO<sub>4</sub>)<sup>2-</sup> tetrahedra having different mean distances of Mo-O bonds are present in  $\beta'$ -RE<sub>2</sub>(MoO<sub>4</sub>)<sub>3</sub> crystals, i.e., type-I, II, and III, three crystallographically independent (MoO<sub>4</sub>)<sup>2-</sup> tetrahedra form successive layers along the *c*-axis [27–30]. Each (MoO<sub>4</sub>)<sup>2-</sup> tetrahedron is discrete, and each oxygen atom in (MoO<sub>4</sub>)<sup>2-</sup> is bonded only to one Mo atom, in addition to either one or two Tb atoms. Recently, MoO<sub>3</sub>-based crystals such as ZnMoO<sub>4</sub> and KLa(MoO<sub>4</sub>)<sub>2</sub> have been reported to be good hosts for Tb<sup>3+</sup>-doping and green emission [31,32]. Peng et al. [20]

<sup>a</sup> e-mail: maalidph@yahoo.co.uk

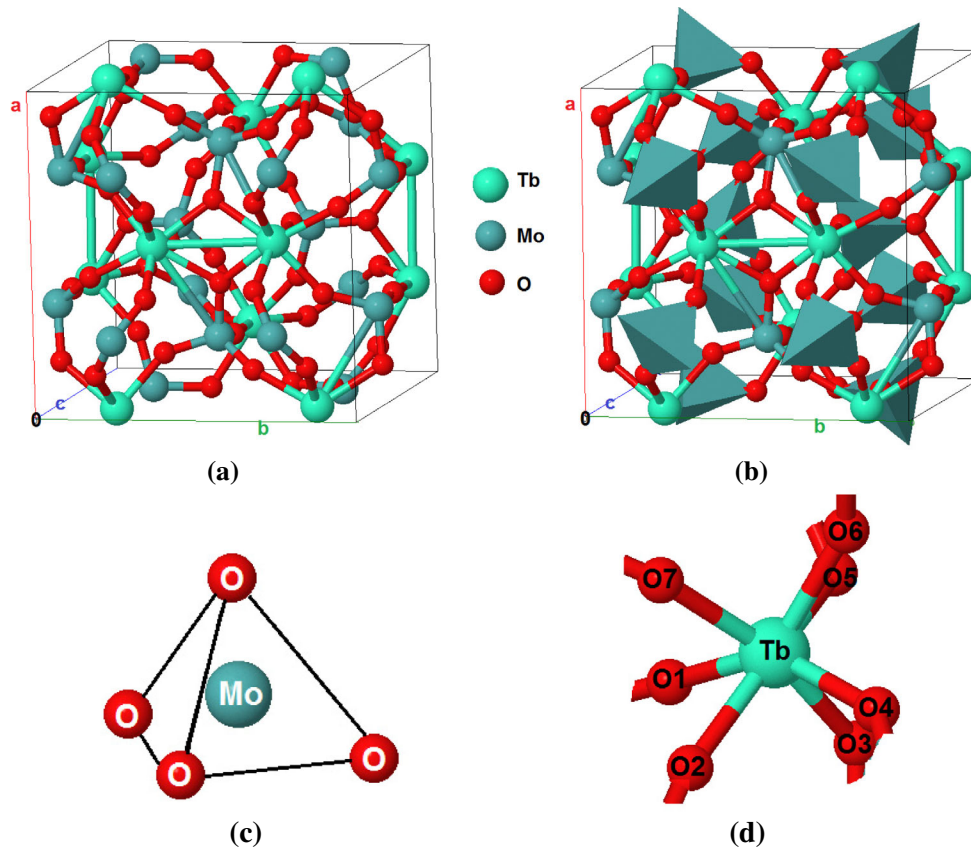


**Fig. 1.** Crystal structure of  $\beta'$ - $\text{Tb}_2(\text{MoO}_4)_3$ ; (a, b) the  $\text{MoO}_4$  tetrahedrons and  $\text{Tb}_7$  polyhedrons are linked by corners; (c)  $\text{MoO}_4$  tetrahedrons in  $\beta'$ - $\text{Tb}_2(\text{MoO}_4)_3$ ; (d)  $\text{TbO}_7$  polyhedrons in  $\beta'$ - $\text{Tb}_2(\text{MoO}_4)_3$ .

have experimentally investigated the optical properties of a novel ferroelectric and ferroelastic multiferroic material  $\text{Tb}_2(\text{MoO}_4)_3$ . They found that the transmission spectrum of  $\text{Tb}_2(\text{MoO}_4)_3$  reflects the band gap of about 3.76 eV and a large absorption peak at 486 nm is observed. They have measured the photoluminescence of the  $\text{Tb}_2(\text{MoO}_4)_3$  and the peaks observed at 490, 540, 580 and 615 nm were attributed to the electronic transitions of  $\text{Tb}^{3+}$  ions. The strongest photoluminescence intensity is excited by the light of 486 nm which is mainly caused by the energy absorption at 486 nm indicated in transmission spectrum.

From above we found that, in order to investigate the ground state properties of  $\beta'$ - $\text{Tb}_2(\text{MoO}_4)_3$ , it is interesting to perform spin-polarized calculation using the density functional theory plus U-Hubbard Hamiltonian. In this report, we would like to reveal the influence of the spin-polarization on the ground state properties of  $\beta'$ - $\text{Tb}_2(\text{MoO}_4)_3$ .

## 2 Details of calculations

The experimental structural geometry of  $\beta'$ - $\text{Tb}_2(\text{MoO}_4)_3$  compound [26] was optimized using the full potential linear augmented plane wave plus the local orbitals (FP-LAPW + lo) method, as implemented in WIEN2k code [33] within the generalized gradient approximation

(PBE -GGA) [34]. The optimized crystal structure of  $\beta'$ - $\text{Tb}_2(\text{MoO}_4)_3$  is depicted in Figure 1. The structure consists of  $\text{MoO}_4$  tetrahedrons and  $\text{Tb}_7$  polyhedrons linked by corners. For oxides and other highly correlated compounds, local density approximation (LDA) and GGA are known to fail in giving the correct ground state. In these systems, the electrons are highly localized. The Coulomb repulsion between the electrons in open shells should be taken into account. As there is no exchange correlation functional that can include this in an orbital independent way, a simpler approach is to add the Hubbard-like on-site repulsion to the Kohn-Sham Hamiltonian. This is known as LDA+U or GGA + U calculations. There are different ways in which this can be implemented. In the present work, we used the method of Anisimov et al. [35] and Liechtenstein et al. [36] where the Coulomb ( $U$ ) and exchange ( $J$ ) parameters are used. From the obtained relaxed geometry the ground state properties were determined using FP-LAPW + lo [34,37,38] within GGA + U (U-Hubbard Hamiltonian). We applied  $U$  on the 4*f* orbital of Tb atoms and the 4*d* orbital of Mo atoms, we have testified several  $U$  values till we reached the energy band gap values that agree well with the experimental results [20,39–41]. The  $U$  values used here are 0.54 Ry and 0.22 Ry for the 4*f* orbital of Tb atoms and the 4*d* orbital of Mo atoms, respectively. The potential for the construction of the basis functions inside the sphere

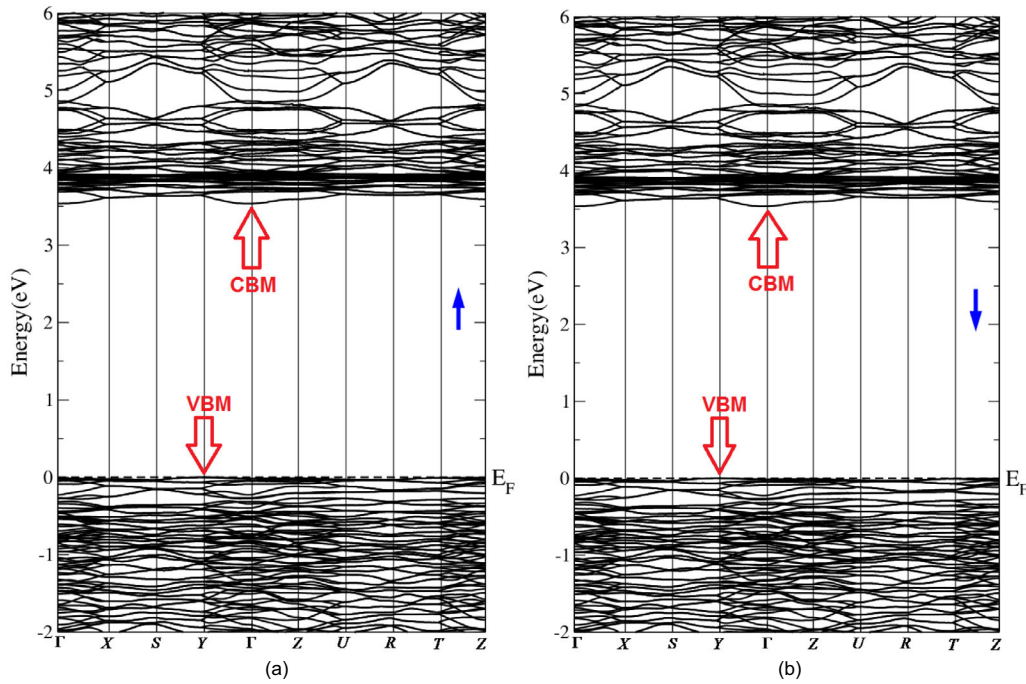


**Fig. 2.** Calculated electronic band structure of  $\beta'$ - $\text{Tb}_2(\text{MoO}_4)_3$ ; (a) spin-up; (b) spin-down.

of the muffin-tin was spherically symmetric, whereas it was constant outside the sphere. Self-consistency is obtained using  $800 \vec{k}$  points in the irreducible Brillouin zone (IBZ). The self-consistent calculations are converged since the total energy of the system is stable within 0.00001 Ry. The electronic band structure and the related properties were performed within  $1728 \vec{k}$  points in the IBZ. It is well known that first-principles calculations are a powerful and useful tool to predict the crystal structure and its properties related to the electron configuration of a material before its synthesis [42–45].

### 3 Results and discussion

#### 3.1 Spin-polarized electronic band structure and density of states

To ascertain the influence of the spin-polarization on the ground state properties of orthorhombic  $\beta'$ - $\text{Tb}_2(\text{MoO}_4)_3$ , the spin-polarized electronic band structure for spin-up ( $\uparrow$ ) and spin-down ( $\downarrow$ ) are calculated, and the results are shown in Figures 2a and 2b. It has been found that for spin-up ( $\uparrow$ ) and spin-down ( $\downarrow$ ) the  $\beta'$ - $\text{Tb}_2(\text{MoO}_4)_3$  compound possesses indirect energy band gap as the valence band maximum (VBM) is located at Y point of the BZ and the conduction band minimum (CBM) is at the center of the BZ. For spin-up ( $\uparrow$ ) and spin-down ( $\downarrow$ ) cases the zero of the energy scale is taken at the top of the valence band. The calculated values of the band gap are equal to 3.61 eV for spin-up ( $\uparrow$ ) and spin-down ( $\downarrow$ ) that is in close agreement with the measured one (3.76 eV) [20,39–41]. It is clear that the electronic band structure for spin-up

( $\uparrow$ ) and spin-down ( $\downarrow$ ) cases present identical structures and, therefore, we can conclude that the spin-polarization has identical influence on the ground state properties of  $\beta'$ - $\text{Tb}_2(\text{MoO}_4)_3$ . In contrast, with  $\alpha$ - $\text{Eu}_2(\text{MoO}_4)_3$  [46],  $\text{Co}_2\text{VAl}$  and  $\text{Co}_2\text{VGa}$  [47] where the electronic band structures for spin-up ( $\uparrow$ ) and spin-down ( $\downarrow$ ) cases are not identical. To ascertain this observation we have presented and explained the necessary ingredients of the calculated total and atom-resolved density of states, as shown in Figures 3a–3g. Figure 3a presents the total density of states (TDOS) for spin-up ( $\uparrow$ ) and spin-down ( $\downarrow$ ) cases which are identical confirming that the spin-polarization has identical influence on the ground state properties of  $\beta'$ - $\text{Tb}_2(\text{MoO}_4)_3$ . For more details, in order to have deep insight into the electronic structure, we have presented the atom-resolved density of states which show identical features for spin-up ( $\uparrow$ ) and spin-down ( $\downarrow$ ). The angular momentum projected density of states (PDOS) helps to identify the angular momentum character of the various structures. Figure 3b explore the contributions of Tb, Mo and O atoms to the electronic density of states of spin-up ( $\uparrow$ ) and spin-down ( $\downarrow$ ) cases of  $\beta'$ - $\text{Tb}_2(\text{MoO}_4)_3$  which are identical. The contributions of Tb-4f and Mo-4d are illustrated in Figure 3c which reveals that both of Tb-4f and Mo-4d govern the CBM, while the O-2p state form the VBM for spin-up ( $\uparrow$ ) and spin-down ( $\downarrow$ ), as shown in Figure 3d. Whereas, the states Tb-6s/5p/4d, Mo-5s/4p and O-2s are very broad, extending from  $-5.0$  eV to 18.0 eV with different contribution for each state but identical contribution for spin-up ( $\uparrow$ ) and spin-down ( $\downarrow$ ) cases, as shown in Figures 3d–3f. It has been noticed that Tb-6s, Mo-5s and O-2s states are strongly hybridized at the VBM, whereas Tb-6s and O-2s states hybridized at the CBM (Fig. 3f). Also, Tb-4d and O-2p states hybridized

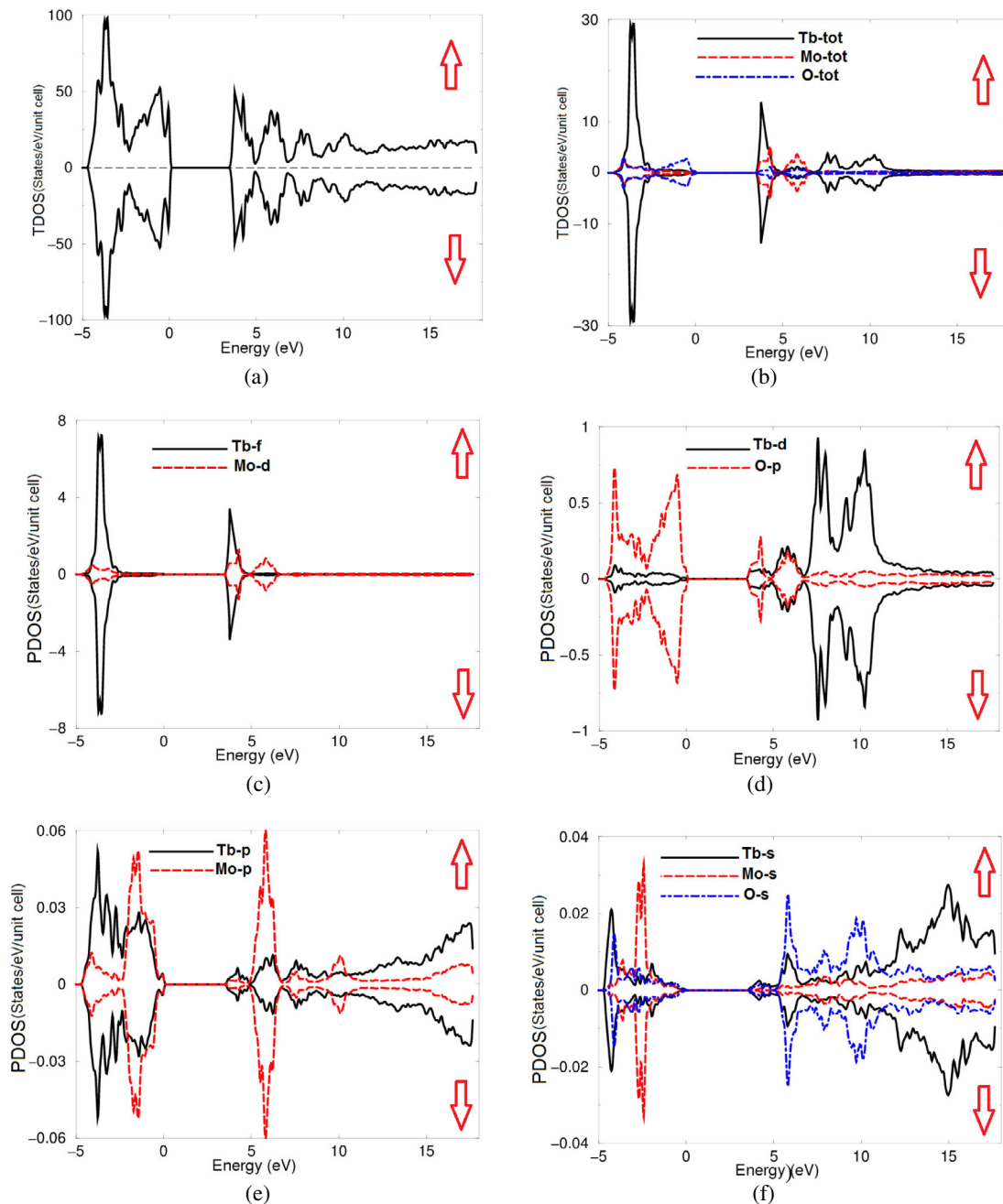


**Fig. 3.** Calculated spin-up/down total and partial density of states of  $\beta'$ - $\text{Tb}_2(\text{MoO}_4)_3$ .

around 5.5 eV, Tb-5p hybridized with Mo-4p at the VBM. The hybridization may lead to the formation of covalent bonds depending on the degree of the hybridization.

To visualize the charge transfer and the chemical bonding characters, the valence band electronic charge density distributions are calculated and analyzed in detail. Figures 4a–4d illustrated the calculated total valence charge density distribution in (1 0 0) and (1 0 1) crystallographic planes for spin-up and spin-down cases. According to Pauling scale, the electro-negativity levels of Tb, Mo and O atoms are 1.1, 2.16 and 3.44, respectively. Therefore, due to the electro-negativity difference between the atoms, some valence electrons are transferred towards O atoms,

as it is clear from the O atom surroundings by uniform blue spheres (indicating the maximal charge accumulation). For both cases (spin up/down), the O atoms of the  $\text{MoO}_4$  tetrahedrons form strong covalent bonds with Mo atom. While the O atoms in  $\text{TbO}_7$  polyhedrons form bonds with weak covalent component, as it is confirmed by the interatomic distances in Table 1 in comparison with the measured values [26], and good agreement was found. We would like to highlight that the crystallographic plane (1 0 0) shows O atoms of the  $\text{TbO}_7$  polyhedrons in  $\beta'$ - $\text{Tb}_2(\text{MoO}_4)_3$  which reveals that the O atoms exhibit weak covalent bonds (see Figs. 4a and 4b). Whereas,

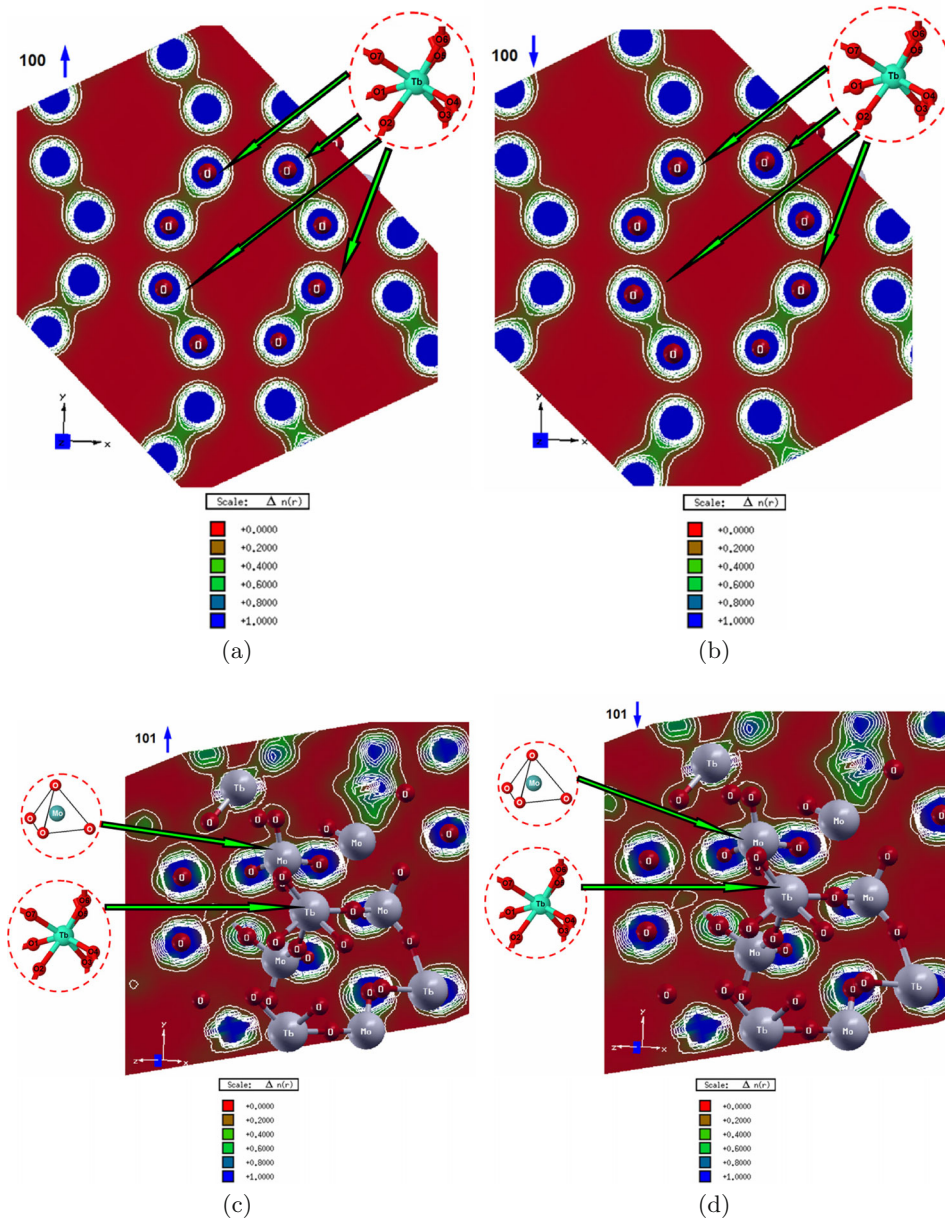


**Fig. 4.** Calculated electronic charge density distribution; (a) the crystallographic plane (1 0 0) for spin-up show O atoms of the  $TbO_7$  polyhedrons in  $\beta'$ - $Tb_2(MoO_4)_3$ ; (b) the crystallographic plane (1 0 0) for spin-down show O atoms of the  $TbO_7$  polyhedrons in  $\beta'$ - $Tb_2(MoO_4)_3$ ; (c) the crystallographic plane (1 0 1) for spin-up show the  $MoO_4$  tetrahedrons and  $TbO_7$  polyhedrons in  $\beta'$ - $Tb_2(MoO_4)_3$ ; (d) the crystallographic plane (1 0 1) for spin-down show the  $MoO_4$  tetrahedrons and  $TbO_7$  polyhedrons in  $\beta'$ - $Tb_2(MoO_4)_3$ .

the crystallographic plane (1 0 1) show the  $MoO_4$  tetrahedrons and  $TbO_7$  polyhedrons in  $\beta'$ - $Tb_2(MoO_4)_3$  and the O atoms of  $MoO_4$  tetrahedrons exhibit strong covalent bonds (see Figs. 4c and 4d).

### 3.2 Complex first-order linear optical dispersion

To obtain more details about the electronic structure and, hence, the ground state properties, the complex first-order linear optical dispersion is calculated for spin-up ( $\uparrow$ ) and

spin-down ( $\downarrow$ ) cases. Figure 5a illustrated the dispersion of the imaginary part of the optical dielectric function for spin-up ( $\uparrow$ ) and spin-down ( $\downarrow$ ) to ascertain the influence of the spin polarization on the optical properties. The first critical points (the absorption edges) for the three components  $\epsilon_2^{xx}(\omega)$  ( $\uparrow$ )( $\downarrow$ ),  $\epsilon_2^{yy}(\omega)$  ( $\uparrow$ )( $\downarrow$ ) and  $\epsilon_2^{zz}(\omega)$  ( $\uparrow$ )( $\downarrow$ ) of the imaginary part of the optical dielectric function along the polarizations directions [1 0 0], [0 1 0] and [0 0 1] are located at 3.61 eV for the spin-up ( $\uparrow$ ) and spin-down ( $\downarrow$ ), confirming our previous observation from Figures 2–4 which reveal that the spin-polarization

**Table 1.** Calculated interatomic distances in MoO<sub>4</sub> tetrahedrons and TbO<sub>7</sub> polyhedrons of  $\beta'$ -Tb<sub>2</sub>(MoO<sub>4</sub>)<sub>3</sub> in comparison with the measured one [26].

Bond	Distance (Å) measured	Distance (Å) calculated	Bond	Distance (Å) measured	Distance (Å) calculated
Tb <sub>1</sub> -O1	2.27(3)	2.26	Mo1-O1	1.80(3)	1.79
Tb <sub>1</sub> -O4	2.31(5)	2.30	Mo1-O3	1.78(3)	1.77
Tb <sub>1</sub> -O4	2.33(5)	2.32	Mo1-O6	1.85(3)	1.85
Tb <sub>1</sub> -O5	2.31(3)	2.30	Mo1-O8	1.82(3)	1.83
Tb <sub>1</sub> -O7	2.59(3)	2.60	Mo2-O2	1.64(3)	1.63
Tb <sub>1</sub> -O10	2.23(3)	2.22	Mo2-O4	1.93(2)	1.92
Tb <sub>1</sub> -O12	2.17(4)	2.16	Mo2-O5	1.78(3)	1.79
Tb <sub>2</sub> -O2	2.42(3)	2.41	Mo2-O7	1.52(3)	1.51
Tb <sub>2</sub> -O3	2.48(3)	2.49	Mo3-O9	1.66(3)	1.67
Tb <sub>2</sub> -O3	2.48(3)	2.49	Mo3-O10	1.68(3)	1.67
Tb <sub>2</sub> -O6	2.29(3)	2.27	Mo3-O11	1.80(3)	1.79
Tb <sub>2</sub> -O8	2.26(3)	2.25	Mo3-O12	1.83(4)	1.81
Tb <sub>2</sub> -O9	2.40(3)	2.39			
Tb <sub>2</sub> -O11	2.20(3)	2.19			

**Table 2.** Calculated  $\varepsilon_1^{xx}(0)$ ,  $\varepsilon_1^{yy}(0)$ ,  $\varepsilon_1^{zz}(0)$ ,  $\delta\varepsilon$ ,  $\omega_p^{xx}$ ,  $\omega_p^{yy}$ ,  $\omega_p^{zz}$ ,  $n^{xx}(\omega)$ ,  $n^{yy}(\omega)$ ,  $n^{zz}(\omega)$  and  $\Delta n(\omega)$  of  $\beta'$ -Tb<sub>2</sub>(MoO<sub>4</sub>)<sub>3</sub> for spin-up ( $\uparrow$ ) and spin-down ( $\downarrow$ ).

	Spin up ( $\uparrow$ )	Spin down ( $\downarrow$ )
$\varepsilon_1^{xx}(0)$	2.345	2.345
$\varepsilon_1^{yy}(0)$	2.351	2.351
$\varepsilon_1^{zz}(0)$	2.436	2.436
$\delta\varepsilon$	-0.037	-0.037
$\omega_p^{xx}$	13.428	13.428
$\omega_p^{yy}$	13.416	13.416
$\omega_p^{zz}$	13.428	13.428
$n^{xx}(\omega)$	1.531	1.531
$n^{yy}(\omega)$	1.533	1.533
$n^{zz}(\omega)$	1.561	1.561
$\Delta n(\omega)$	0.029	0.029

has identical influence on the ground state properties of  $\beta'$ -Tb<sub>2</sub>(MoO<sub>4</sub>)<sub>3</sub>. Following the optical selection rules, the absorption edges occurs due to the transitions between the states just below and above Fermi level ( $E_F$ ).

The first spectral structure in  $\varepsilon_2^{xx}(\omega)$  ( $\uparrow$ )( $\downarrow$ ),  $\varepsilon_2^{yy}(\omega)$  ( $\uparrow$ )( $\downarrow$ ) and  $\varepsilon_2^{zz}(\omega)$  ( $\uparrow$ )( $\downarrow$ ) occurs mainly due to the transitions between O-2p and Tb-4f states while the second spectral structure occurs due to the allowed optical transitions between O-2p, Mo-5s/4p, Tb-5p/4d states of the valence bands and O-2s/2p, Tb-4d, Mo-4p/4d of the conduction bands. The tail occurs due to the transitions between O-2p, Tb-4d/4f, Mo-4p of the VBs and O-2p, Tb-4d, Mo-4p of the CBs. This spectral structure exhibits the lossless regions.

The real parts along the polarizations directions [1 0 0], [0 1 0] and [0 0 1], as derived from the imaginary part using Kramers-Kronig transformation [48], are presented in Figure 5b. We found that the calculated values of  $\varepsilon_1^{xx}(0)$ ,  $\varepsilon_1^{yy}(0)$  and  $\varepsilon_1^{zz}(0)$  are identical for spin-up ( $\uparrow$ ) and spin-down ( $\downarrow$ ), as shown in Table 2. Based on Penn model [49] we can derive the value of the energy band gap from  $\varepsilon_1^{xx}(0)$ ,  $\varepsilon_1^{yy}(0)$  and  $\varepsilon_1^{zz}(0)$ . Penn proposed a relation

between  $\varepsilon(0)$  and  $E_g$ ,  $\varepsilon(0) \approx 1 + (\hbar\omega_P/E_g)^2$ , where  $E_g$  is an averaged energy gap. It is clear that  $\varepsilon(0)$  is inversely proportional with  $E_g$ . Since the  $\varepsilon_1^{xx}(0)$ ,  $\varepsilon_1^{yy}(0)$  and  $\varepsilon_1^{zz}(0)$  values are the same for spin-up ( $\uparrow$ ) and spin-down ( $\downarrow$ ), the obtained values of energy gaps following Penn model are the same and, hence, the spin-polarization has identical influence on the ground state properties of  $\beta'$ -Tb<sub>2</sub>(MoO<sub>4</sub>)<sub>3</sub>. In addition, we have calculated the uniaxial anisotropy  $\delta\varepsilon = [(\varepsilon_0^{II} - \varepsilon_0^I)/\varepsilon_0^{tot}]$  [50] for the spin-up and spin-down cases at static limit, as listed in Table 2. The values indicate the existence of considerable anisotropy. It is clear that  $\beta'$ -Tb<sub>2</sub>(MoO<sub>4</sub>)<sub>3</sub> possesses negative uniaxial anisotropy. Another evidence is that the spin-polarization has identical influence on the ground state properties of  $\beta'$ -Tb<sub>2</sub>(MoO<sub>4</sub>)<sub>3</sub>. There are other features in the optical spectrum of  $\varepsilon_1^{xx}(\omega)$  ( $\uparrow$ )( $\downarrow$ ),  $\varepsilon_1^{yy}(\omega)$  ( $\uparrow$ )( $\downarrow$ ) and  $\varepsilon_1^{zz}(\omega)$  ( $\uparrow$ )( $\downarrow$ ), such as plasmon oscillations, which are associated with inter-band transitions. The plasmon maximum  $\omega_p^{xx}(\omega)$  ( $\uparrow$ )( $\downarrow$ ),  $\omega_p^{yy}(\omega)$  ( $\uparrow$ )( $\downarrow$ ) and  $\omega_p^{zz}(\omega)$  ( $\uparrow$ )( $\downarrow$ ) is usually the most intense feature in the spectrum and this is at energy where  $\varepsilon_1^{xx}(\omega)$  ( $\uparrow$ )( $\downarrow$ ),  $\varepsilon_1^{yy}(\omega)$  ( $\uparrow$ )( $\downarrow$ ) and  $\varepsilon_1^{zz}(\omega)$  ( $\uparrow$ )( $\downarrow$ ) crosses zero which is associated with the existence of plasma oscillations. The plasma frequency (energy) is calculated and presented in Table 2 which shows that these values are identical for spin-up and spin-down.  $\beta'$ -Tb<sub>2</sub>(MoO<sub>4</sub>)<sub>3</sub> exhibit low reflectivity almost 20% along the whole energy range, as illustrated in Figure 5e. The reflectivity minima occurs around 12.0 eV confirming the occurrence of collective plasmon resonance which represents the lossless regions.

In addition, we have calculated the refractive indices  $n^{xx}(\omega)$ ,  $n^{yy}(\omega)$  and  $n^{zz}(\omega)$  for spin-up and spin-down, as shown in Figure 5f. The values of the refractive at the static limit are listed in Table 3. The refractive indices have direct relation with the energy band gap ( $n = \sqrt{\varepsilon}$ ) and, therefore, we can estimate the value of the energy band gap from calculated values of the refractive indices. From the calculated values of the refractive indices we can derive the values of the birefringence.

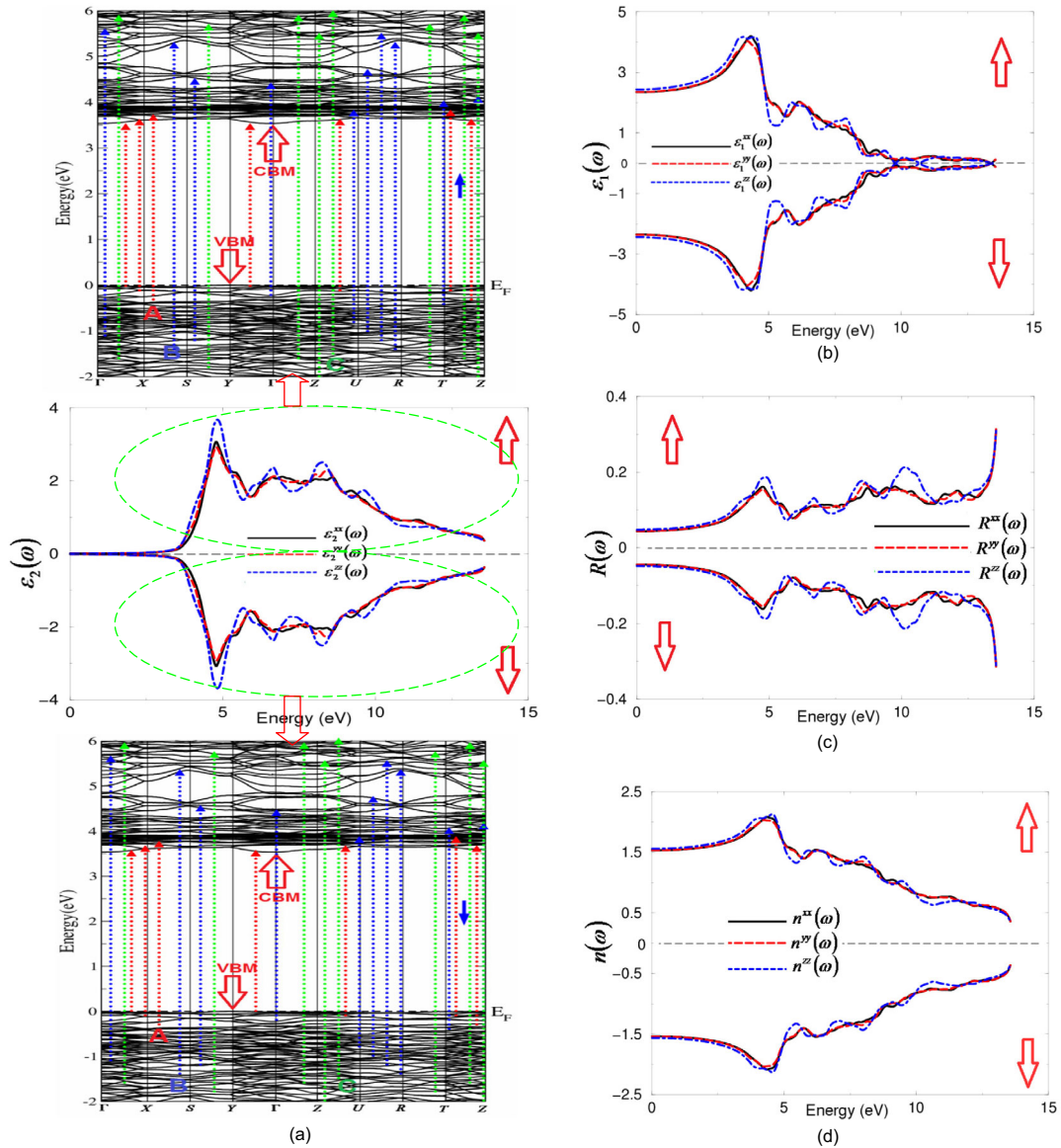


**Fig. 5.** (a) Upper panel: the optical transitions depicted on a generic band structure of  $\beta'$ -Tb<sub>2</sub>(MoO<sub>4</sub>)<sub>3</sub> for spin-up. Middle panel: calculated  $\epsilon_2^{xx}(\omega)$  (dark solid curve-black color online),  $\epsilon_2^{yy}(\omega)$  (light solid curve-blue color online) and  $\epsilon_2^{zz}(\omega)$  (light solid curve-blue color online) spectra for spin-up/down. Lower panel: the optical transitions depicted on a generic band structure of  $\beta'$ -Tb<sub>2</sub>(MoO<sub>4</sub>)<sub>3</sub> for spin-down; (b) calculated  $\epsilon_1^{xx}(\omega)$  (dark solid curve-black color online),  $\epsilon_1^{yy}(\omega)$  (light dashed curve-red color online) and  $\epsilon_1^{zz}(\omega)$  (light solid curve-blue color online) spectra for spin-up/down; (c) Calculated  $R^{xx}(\omega)$  (dark solid curve-black color online),  $R^{yy}(\omega)$  (light dashed curve-red color online) and  $R^{zz}(\omega)$  (light solid curve-blue color online) spectra for spin-up/down; (d) Calculated  $n^{xx}(\omega)$  (dark solid curve-black color online),  $n^{yy}(\omega)$  (light dashed curve-red color online) and  $n^{zz}(\omega)$  (light solid curve-blue color online) spectra for spin-up/down.

From above it has been noticed that the three optical tensor components exhibit a considerable anisotropy among each other.

## 4 Conclusions

The all-electron full potential linear augmented plane wave (FP-LAPW + lo) method within the generalized gradient approximation plus the Hubbard Hamiltonian (GGA + U) was used to calculate the spin polarized

electronic band structure, density of states, the chemical bonding and the optical properties of  $\beta'$ -Tb<sub>2</sub>(MoO<sub>4</sub>)<sub>3</sub>. We have applied  $U$  on  $4f$  orbital of Tb atoms and  $4d$  orbital of Mo atoms. The calculations show that  $\beta'$ -Tb<sub>2</sub>(MoO<sub>4</sub>)<sub>3</sub> is indirect band gap semiconductor for spin-up and spin-down cases. We have calculated total valence charge density distribution in (1 0 0) and (1 0 1) crystallographic planes for spin-up and spin-down cases. The calculated bond lengths show very good agreements with the values derived by structural analysis. The optical properties show the existence of a lossless region and considerable

anisotropy. It has been found that the  $\beta'$ -Tb<sub>2</sub>(MoO<sub>4</sub>)<sub>3</sub> crystal exhibits negative uniaxial anisotropy.

The result was developed within the CENTEM project, Reg. No. CZ.1.05/2.1.00/03.0088, cofunded by the ERDF as part of the Ministry of Education, Youth and Sports OP RDI programme and, in the follow-up sustainability stage, supported through CENTEM PLUS (LO1402) by financial means from the Ministry of Education, Youth and Sports under the “National Sustainability Programme I”. Computational resources were provided by MetaCentrum (LM2010005) and CERIT-SC (CZ.1.05/3.2.00/08.0144) infrastructures.

## References

- H.J. Borhardt, P.E.J. Bierstedt, Appl. Phys. **38**, 2057 (1967)
- A.K. Tripathi, H.B.J. Lal, Phys. Soc. Jpn **49**, 1896 (1980)
- V.A. Efremov, Russ. Chem. Rev. **59**, 627 (1990)
- V. Dmitriev, V. Sinitsyn, R. Dilanian, D. Machon, A. Kuznetsov, E. Ponyatovsky, G. Lucazeau, H.P.J. Weber, Phys. Chem. Solids **64**, 307 (2003)
- B.G. Bazarov, R.F. Klevtsova, O.D. Chimitova, I.A. Glinskaya, K.N. Fedorov, Y.L. Tushinova, Z.G. Bazarova, Russ. J. Inorg. Chem. **51**, 800 (2006)
- Z.G. Xia, D.M.J. Chen, Am. Ceram. Soc. **93**, 1397 (2010)
- M. Mączka, A. Majchrowski, I.V. Kityk, Vib. Spectrosc. **64**, 158 (2013)
- O.D. Chimitova, V.V. Atuchin, B.G. Bazarov, M.S. Molokeyev, Z.G. Bazarova, Proc. SPIE **8771**, 87711A (2013)
- J. Hanuza, L. Macalik, K.J. Hermanowicz, Mol. Struct. **319**, 17 (1994)
- L.J. Macalik, Alloys Compd. **341**, 226 (2002)
- A. Kato, S. Oishi, T. Shishido, M. Yamazaki, S.J. Iida, Phys. Chem. Solids **66**, 2079 (2005)
- O.D. Chimitova, B.G. Bazarov, R.F. Klevtsova, A.G. Anshits, K.N. Fedorov, A.V. Dubentsov, T.A. Vereshchagina, Y.L. Tushinova, L.A. Glinskaya, Z.G. Bazarova, L.I. Gongorova, J. Struct. Chem. **51**, 173 (2010)
- J.F. Tang, Y.J. Chen, Y.F. Lin, X.H. Gong, J.H. Huang, Z.D. Luo, Y.D.J. Huang, Opt. Soc. Am. B **27**, 1769 (2010)
- V.V. Atuchin, V.G. Grossman, S.V. Adichtchev, N.V. Surovtsev, T.A. Gavrilova, B.G. Bazarov, Opt. Mater. **34**, 812 (2012)
- C.S. Lim, Asian J. Chem. **24**, 5662 (2012)
- V.V. Atuchin, O.D. Chimitova, S.V. Adichtchev, B.G. Bazarov, T.A. Gavrilova, M.S. Molokeyev, N.V. Surovtsev, Zh.G. Bazarova, Mater. Lett. **106**, 26 (2013)
- S. Mielcarek, Z. Tylczyński, Z. Trybuła, S. Łoś, B. Mroz, Cryst. Res. Technol. **40**, 1146 (2005)
- Guipeng Cai, Jiyang Wang, Huaijin Zhang, Cryst. Res. Technol. **44**, 1001 (2009)
- K. Nassau, H.J. Levinstein, G.M. Loiacono, J. Phys. Chem. Solids **26**, 1805 (1965)
- Song Peng, Wei Cai, Xiaofei Wang, Yi Kan, Fengzhen Huang, Min Xu, Huaijin Zhang, Jiyang Wang, Xiaomei Lu, Jinsong Zhu, Ferroelectrics **410**, 69 (2010)
- H.J. Borhardt, P.E. Bierstedt, J. Appl. Phys. **18**, 2057 (1967)
- E.T. Keve, S.C. Abrahams, K. Nassau, A.M. Glass, Solid State Commun. **8**, 1517 (1970)
- E.T. Keve, S.C. Abrahams, J.L. Bernstein, J. Chem. Phys. **54**, 3185 (1971)
- S.C. Abrahams, C. Svensson, J.L. Bernstein, J. Chem. Phys. **72**, 4278 (1980)
- C. Svensson, S.C. Abrahams, J.L. Bernstein, J. Chem. Phys. **71**, 5191 (1979)
- V.V. Atuchin, A.S. Aleksandrovsky, O.D. Chimitova, A.S. Krylov, M.S. Molokeyev, B.G. Bazarov, J.G. Bazarova, Zhiguo Xia, Opt. Mater. **36**, 1631 (2014)
- E.T. Keve, S.C. Abrahams, J.L. Bernstein, J. Chem. Phys. **54**, 3185 (1971)
- F.G. Ulman, B.J. Holden, B.N. Gauguly, J.R. Hardy, Phys. Rev. B **8**, 2991 (1973)
- S.S. Saleem, G. Arulhas, H.D. Bist, J. Solid State Chem. **48**, 77 (1983)
- L. Guy, M. Denis, J. Raman Spectrosc. **37**, 189 (2006)
- H. Ida, K. Shinozaki, T. Honma, K. Oh-ishi, T. Komatsu, J. Solid State Chem. **196**, 384 (2012)
- M. Imaoka, J. Ceram. Soc. Jpn **69**, 282 (1961)
- P. Blaha, K. Schwarz, G.K.H. Madsen, D. Kvasnicka, J. Luitz, WIEN2k, An augmented plane wave plus local orbitals program for calculating crystal properties (Vienna University of Technology, Austria, 2001)
- J.P. Perdew, S. Burke, M. Ernzerhof, Phys. Rev. Lett. **77**, 3865 (1996)
- V.I. Anisimov, I.V. Solvyev, M.A. Korotin, M.T. Czyzyk, C.A. Sawatzky, Phys. Rev. B **48**, 16929 (1993)
- A.I. Liechtenstein, V.I. Anisimov, J. Zaanen, Phys. Rev. B **52**, R5467 (1995)
- O.K. Andersen, Phys. Rev. B **12**, 3060 (1975)
- J.P. Perdew, Y. Wang, Phys. Rev. B **45**, 13244 (1992)
- B.K. Ponomarev, B.S. Red'kin, A.G.M. Jansen, P. Wyder, H. Wiegmann, E. Steep, Phys. Solid State **50**, 1495 (2008)
- M. Xu, Y.G. Yu, H.J. Zhang, J.Y. Wang, J. Rare Earths **27**, 192 (2009)
- G.P. Cai, J.Y. Wang, H.J. Zhang, Cryst. Res. Technol. **44**, 1001 (2009)
- Y. Saeed, S. Nazir, A. Shaukat, A.H. Reshak, J. Magn. Magn. Mater. **322**, 3214 (2010)
- M.B. Kanoun, A.H. Reshak, N.K.-Bouayed, S.G.-Said, J. Magn. Magn. Mater. **324**, 1397 (2012)
- H.S. Saini, M. Singh, A.H. Reshak, M.K. Kashyap, J. Magn. Magn. Mater. **331**, 1 (2013)
- A.H. Reshak, H. Kamarudin, Z.A. Alahmed, S. Auluck, J. Chyský, J. Magn. Magn. Mater. **361**, 206 (2014)
- A.H. Reshak, Z.A. Alahmed, J. Bila, V.V. Atuchin, B.G. Bazarov, O.D. Chimitova, M.S. Molokeyev, I.P. Prosvirin, A.P. Yelisseyev, J. Phys. Chem. C **120**, 10559 (2016)
- A.H. Reshak, RSC Advances **6**, 54001 (2016)
- F. Wooten, *Optical Properties of solids* (Academic Press, New York, London, 1972)
- D.R. Penn, Phys. Rev. B **128**, 2093 (1962)
- G.D. Boyd, H. Kasper, J.H. McFee, IEEE J. Quantum Electron. **7**, 563 (1971)